HARNESSING ORBITAL ENERGY WITH BARE TAPE-LIKE ELECTRODYNAMIC TETHERS FOR EFFICIENT SPACE DEBRIS MITIGATION

Livia Marciano(1), Behrad Vatankhahghadim(1), Gonzalo Sánchez Arriaga(1), and Sven G. Bilén(2)

(1)*Universidad Carlos III de Madrid, Email: {livia.marciano, behrad.vatankhahghadim, gonzalo.sanchez }@uc3m.es*
(2)*The Pennsylvania State University, Email: {sbilen}@psu.edu*

ABSTRACT

Electrodynamic tethers (EDTs) have a unique attribute that distinguishes them from any other in-orbit propulsion technology: they can convert orbital energy into electrical energy as they deorbit space debris from Low Earth Orbit. The harvested energy can be used immediately or stored to be utilized later. This study explores energy-repurposing cases with the goal of incentivizing space sustainability and opening new market opportunities. The work starts by integrating DISCOS and Space-track databases. The combined database is then filtered to identify the most promising scenarios in terms of object removal effectiveness, taking into account the orbits addressable by EDTs and the total harvestable energy. A simulation of such scenarios, which involve orbits with a 35° inclination and objects weighing 300–500 kg, shows that a 1–2-km-long EDT can deorbit from an 800-km altitude within a few months, generating tens to hundreds of watts continuously during the deorbiting process.

Keywords: Electrodynamic tethers, Active debris removal, Harvesting power, Low Earth Orbit, Energy repurposing.

1. INTRODUCTION

To address the challenge of space debris remediation, post-mission disposal (PMD) and active debris removal (ADR) emerge as potential solutions. For both scenarios, EDTs have been proposed as a promising propellantless and active/passive technology for space debris removal [7]. Additionally, a bare EDT system in LEO can convert orbital potential energy into electrical energy [14], allowing for energy repurposing [9]. This is an interesting characteristic of EDTs because any value added by the deorbit technology can act as an incentive to drive the PMD and ADR markets. For instance, if the power provided by the EDT is used to feed a payload, the payload owner may contribute to financing the PMD or ADR mission. The dual application of EDTs for propulsion and power generation has also been proposed for Jovian missions [8, 15, 1].

The objective of this work is to identify specific scenarios for the actual population of space debris that can benefit from the dual application of EDTs as a deorbiting and power generation technology, to support the preliminary design of the EDT system, and determine the performance. An example is the ADR scenarios in which an EDT deorbit device together with a payload is attached to a space debris and the EDT deorbits them while providing power to the payload. Recent advancements in on-orbit servicing technologies and EDTs suggest that such a possibility may be feasible in the next few years. For instance, a 20-kg and 12U autonomous deorbit device based on a tape-like EDT is expected to be demonstrated in orbit in 2026 [11]. This type of EDT system has the appropriate characteristics (geometry and type of cathode) to provide good deorbiting performance while providing power for onboard use.

When addressing the design of EDT systems for such a two-fold use, one should optimize the impedance to maximize the harvested power while maintaining good deorbit performance [13, 14, 16]. In some extreme cases, such as those with small or large ohmic losses and negligible cathode bias, useful analytical formulae for the optimum impedance, the average current, and the power can be found [14, 1]. This study retains the effect of the hollow cathode potential drop and does not make any assumption about the ohmic effect.

This work is structured as follows. Section 2 presents the database used to identify interesting scenarios for dual-mode EDTs. Section 3 explains the methodology for estimating the harvested power and deorbiting performance. A semi-analytical model is introduced and the optimal impedance for maximizing power extraction is investigated. The model is used to find the performance (deorbit time and harvested power) for the selected scenarios as a function of the tether length. Section 4 summarizes the findings and outlines future research directions.

2. SELECTION OF PROMISING SCENARIOS

This section is focused on identifying potential targets for EDT applications by analyzing objects—both orbiting debris and satellites—within a mass range between

30 kg and one tonne and at altitudes between 400 and 800 km. Although EDTs can operate at higher altitudes and with heavier objects, the analysis was focused on scenarios that are sensible in the short time. As part of the study, a comprehensive database of objects was created. As shown below, this database can facilitate market analysis and support technology development by characterizing the orbital and physical properties of these objects.

To build this database, two primary sources were integrated, as neither the information about the objects' characteristics nor their positions in space were available for all types of objects in the same database. The first source is DISCOSweb [4], managed by the European Space Agency (ESA), which provides detailed information on over 40,000 space objects, including their physical characteristics (mass, dimensions) and operators. Data retrieval utilized an Application Programming Interface (API) [5] and Python scripts to filter the objects based on mass and altitude. Challenges include missing mass information for certain debris objects, which was addressed by modifying the filters and retrieving data based on object classes: Other Debris, Other Mission Related Object, Payload, Payload Debris, Payload Fragmentation Debris, Payload Mission Related Object, Rocket Body, Rocket Debris, Rocket Fragmentation Debris, Rocket Mission Related Object, and Unknown. The result of this data-gathering process, the information stored for each object (following the nomenclature of DISCOSweb) includes: Name, COSPAR ID[1], SATNO (Satellite Number), Object Class, Predicted Decay Date, Mass, Shape, Height, Span, Width, Minimum Cross Section, Average Cross Section, Maximum Cross Section, and Operator.

The second source is SpaceTrack [18], which provides up-to-date orbital data. However, the information in SpaceTrack for the objects is categorised in two different parts with two different formats. One is derived from a dataset containing the most recent element set ("elset"), which corresponds to the most recent TLEs for every payload in LEO that had received an update within the past 30 days. The second part is sourced from a Comma-Separated Values (CSV) file containing data of objects currently in orbit as well as those that previously orbited the Earth. As explained below, due to this characeristic of SpaceTrack, our database is also split into two categories.

The two datasets from DISCOS and SpaceTrack were subsequently combined using the COSPAR ID as the shared parameter. This integration process produces two comprehensive datasets of objects in LEO. One dataset includes active payloads and unknown objects, and the other dataset contains rocket bodies and debris. This nomenclature of the categories follows that used by DISCOS. The two datasets include both physical and orbital properties, enabling customized filtering for specific analysis needs. Duplicate entries were reviewed and eliminated, and the results were cross-checked against ESA's published data [6] to ensure accuracy.

The final database does not contain duplicated objects and it only includes objects that are currently orbiting the Earth. For convenience, the Starlink constellation, which distorts the actual distribution of other objects due to their large number of satellites, has been excluded from the following analyses. Nonetheless, they can also be target objects for ADR missions with EDTs. The first type of analysis focused on the spatial distribution of the objects. Figure 1 shows all objects (active payloads and debris) within an altitude range of 400 to 800 km. The data are classified into mass ranges and inclination ranges within each bar. Although a majority of objects are located at high inclinations, a good number of objects with masses around 60, 300, and 720 kg, are found at low and mid-inclinations. For EDTs aligned with the local vertical, orbits with low and medium inclinations are more favorable because of the larger motional electric field component along the EDT direction. They can also be used in Sun-synchronous orbits [3], but this is a harder scenario for simultaneous deorbiting and power harvesting. Spinning EDTs, not considered in this work, may offer a better solution for power harvesting at highly inclined orbits.

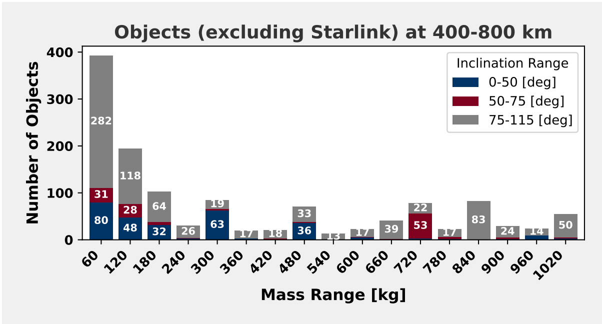

Figure 1. Number of objects with masses between 30 and 1000 kg, excluding Starlink (last updated November 2024).

The total amount of energy that could be potentially harvested by deorbiting all the objects shown in Figure 1 is huge. For each of them, we can compute the difference between the orbital energy in their actual orbital radius (r_0) and a hypothetical final radius (r_{f}). Since for the vast majority of the objects the eccentricity is very small, such a difference reads

$$\Delta E = -\frac{\mu_{\mathrm{E}} m}{2}\left(\frac{1}{r_0} - \frac{1}{r_{\mathrm{f}}}\right), \qquad (1)$$

where μ_{E} is the Earth gravitational parameter and m is the mass of the object. Figure 2 shows ΔE versus the object's mass when a final radius of $r_{\mathrm{f}} = 300$ km is considered. Instead of the inclination as in Figure 1, here different colours are used to separate objects with different initial altitudes (see the legend). The total change in orbital energy for each mass range is indicated at the top of each bar, while the values within each bar represent the energy for each initial altitude within that specific mass range.

[1] International identifier assigned to artificial objects in space

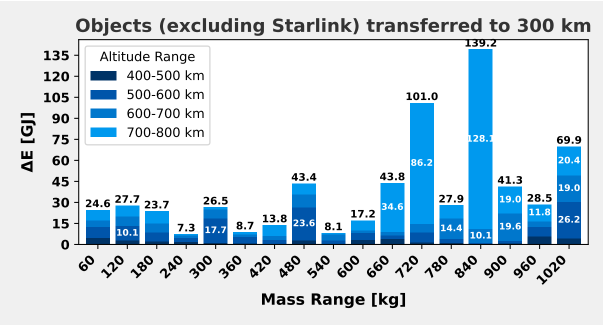

Figure 2. Orbital energy difference of objects between their current orbits and a 300-km altitude orbit, excluding Starlink (last update November 2024). Only objects with mass and altitude in the ranges 30–1000 kg and 400–800 km are considered.

Remarkably, the total ΔE is on the order of hundreds gigajoules (GJ), representing a significant amount of energy that could potentially be transformed into electric power using EDTs. However, only a fraction of this energy can be converted into usable onboard electrical power because the EDT has an orbital-to-electrical power conversion efficiency lower than one. Part of the orbital energy is transferred to Earth's rotational kinetic energy, dissipated by the Joule effects and transferred to the ambient plasma in the form of waves [12]. The subsequent section introduces a model to compute the harvested power for some specific scenarios.

3. A MODEL FOR FINDING THE HARVESTED POWER IN DEORBITING MISSIONS

3.1. Dynamic model

This subsection presents a simple model to compute the deorbit time of a spacecraft of cross-sectional area A_s attached to an EDT aligned with the local vertical. Although the model has been used in several past works on EDTs [17], we summarize here its main elements. The tether, a tape of length L_t, width w_t, and thickness h_t, is bare and the cathodic contact with the ambient plasma is achieved by using a hollow cathode that can emit any current at the cost of a potential drop $V_C < 0$. Since this work is focused ion deorbiting and power harvesting, the model considers an impedance of resistance R located between the EDT and the cathode. In a real system, such an impedance should be substituted by an electronics board that would handle the power. For instance, the power provided by the tether could be used to refill batteries that would feed a payload. Figure 3 shows a sketch of the system with the EDT, the impedance and the cathode.

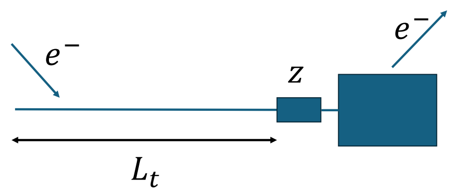

Figure 3. Sketch of an EDT with 1 cathodes and the impedance (R) between the EDT and the cathode.

The spacecraft and the EDT are modeled as a single point mass M_s. The Lorentz force and the aerodynamic drag on the spacecraft and the EDT are the main perturbation forces. The equation of motion then reads

$$M_s \frac{d\boldsymbol{v}}{dt} = -\frac{\mu_E M_s}{r^3}\boldsymbol{r} + \int_0^L I(x)\boldsymbol{u}_t \times \boldsymbol{B} dx - \frac{C_D}{2}\rho_a S v \boldsymbol{v}$$
$$\approx -\frac{\mu_E M_s}{r^3}\boldsymbol{r} + L_t I_{av} \boldsymbol{u}_t \times \boldsymbol{B} - \frac{C_D}{2}\rho_a S v \boldsymbol{v} \tag{2}$$

where C_D is the drag coefficient (assumed to be equal of the spacecraft and the EDT), ρ_a is the atmospheric density and

$$S = A_s + \frac{2w_t}{\pi} L \tag{3}$$

is the total cross-sectional area of the spacecraft and the EDT. In Eq. (2), we assumed that the aerodynamic velocity coincides with the orbital velocity, and the geomagnetic field $\boldsymbol{B}$ is constant along the EDT. We also introduced the position ($\boldsymbol{r}$) and velocity ($\boldsymbol{v} = d\boldsymbol{r}/dt$) vectors of the spacecraft, the current along the tether ($\boldsymbol{I} = I(x)\boldsymbol{u}_t$), and the average current

$$I_{av} = \frac{1}{L_t}\int_0^L I(x)dx. \tag{4}$$

For a bare EDT, the average current satisfies [14]

$$\frac{I_{av}}{\sigma_t A_t E_m} \equiv i_{av}\left(\phi_C, \xi_t, \mathrm{z}\right), \tag{5}$$

where the three dimensionless parameters in the right-hand side are given by

$$\phi_C \triangleq \frac{V_c}{E_m L^*}, \quad \xi_t \triangleq \frac{L_t}{L^*}, \quad \mathrm{z} \triangleq \frac{R A_t \sigma_t}{L^*}, \tag{6}$$

representing the normalized voltage drop at the cathode, normalized length, and normalized impedance, respectively, and the characteristic length is given by

$$L^* = \left(\frac{2A_t}{p_t}\right)^{\frac{2}{3}} \left(\frac{9\pi^2 m_e \sigma_t^2 E_m}{128 e^3 N_0^2}\right)^{\frac{1}{3}} \tag{7}$$

with R the physical resistance, A_t, p_t and σ_t denoting the cross-sectional area of the tether, its perimeter and conductivity, respectively, m_e is the electron mass, e is the elementary charge, N_0 the plasma number density, $E_\mathrm{m} \equiv (\boldsymbol{v}_\mathrm{rel} \times \boldsymbol{B}) \cdot \boldsymbol{u}_\mathrm{t}$ the motional electric field, and $\boldsymbol{v}_\mathrm{rel}$ the tether-to-plasma relative velocity.

Assuming that the Lorentz force is small and the spacecraft follows a sequence of quasi-circular orbits with $v \approx \sqrt{\mu_\mathrm{E}/r}$, taking the dot product of Eq. (2) with $\mathbf{v}$ gives

$$\frac{dr}{dt} = -\frac{2r^2}{\mu_\mathrm{E} M_\mathrm{s}} \left[E_\mathrm{m}^2 \sigma_\mathrm{t} A_\mathrm{t} L_\mathrm{t} i_\mathrm{av} + \frac{1}{2} C_\mathrm{D} \rho_\mathrm{a} S \left(\frac{\mu_\mathrm{E}}{r} \right)^{3/2} \right]. \tag{8}$$

The three variables E_m, N_0, and ρ_a appearing in Eq. (7) and in Eq. (8) depend on both position and time. In our simplified model, we average them over several orbits to obtain values that depend only on the orbital altitude H and inclination i. To determine the profiles to be averaged for both N_0 and ρ_a, the mission analysis software BETsMA v2.0 [10] was used. BETsMA v2.0 incorporates the International Reference Ionosphere (IRI) model for N_0 and the NRLMSISE-00 model for ρ_a. As an example of this averaging process, we consider the plasma density

$$\bar{N}_0(H, i) \equiv \frac{1}{2N\pi} \int_0^{2N\pi} N_0 \, d\nu \tag{9}$$

with N denoting a large integer that represents the number of orbits used to average. A similar procedure was used to find $\bar{\rho}_\mathrm{a}(H, i)$.

Regarding the motional electric field $E_\mathrm{m} = (\boldsymbol{v}_\mathrm{rel} \times \boldsymbol{B}) \cdot \boldsymbol{u}_\mathrm{t}$, we considered a tether aligned with the local vertical, i.e., $\boldsymbol{u}_\mathrm{t} = \boldsymbol{r}/r$, a circular orbit, and a tilted dipole model of the magnetic field. Therefore, we have

$$\boldsymbol{r} = r \left(\cos\nu \, \boldsymbol{i}_\mathrm{I} + \cos i \sin\nu \, \boldsymbol{j}_I + \sin i \sin\nu \, \boldsymbol{k}_\mathrm{I} \right), \tag{10}$$

$$\boldsymbol{v} = v \left(-\sin\nu \, \boldsymbol{i}_\mathrm{I} + \cos i \cos\nu \, \boldsymbol{j}_\mathrm{I} + \sin i \cos\nu \, \boldsymbol{k}_\mathrm{I} \right), \tag{11}$$

$$\frac{\boldsymbol{B}}{B_0} = -\left(\frac{R_\mathrm{E}}{r} \right)^3 \left[\frac{3}{2} \sin i \sin(2\nu) \, \boldsymbol{i}_\mathrm{I} + \frac{3}{2} \sin(2i) \sin^2\nu \, \boldsymbol{j}_\mathrm{I} - \left(1 - 3\sin^2 i \sin^2\nu \right) \boldsymbol{k}_\mathrm{I} \right], \tag{12}$$

where R_E is the Earth radius and B_0 is the mean magnetic field at the equator. We also introduced the unit vectors $\boldsymbol{i}_\mathrm{I}$, $\boldsymbol{j}_\mathrm{I}$, and $\boldsymbol{k}_\mathrm{I}$ along the axes of an inertial frame with its origin at the centre of the Earth and its z-axis along the axis of rotation of the Earth, which is assumed to be normal to the equatorial plane (spanned by $\boldsymbol{i}_\mathrm{I}$ and $\boldsymbol{j}_\mathrm{I}$)

After this averaging process, the deorbit time is computed by integrating Eq. (8) to yield

$$T_\mathrm{F} = \int_{H_\mathrm{F}}^{H_0} \frac{\mu_E M_\mathrm{s} dH}{r^2 \left[2\bar{E}_\mathrm{m}^2 L_\mathrm{t} A_\mathrm{t} \sigma_\mathrm{t} i_\mathrm{av} + C_\mathrm{D} \bar{\rho}_\mathrm{a} S \left(\frac{\mu_E}{r} \right)^{3/2} \right]} \tag{13}$$

and the average values of N_0 and E_m, namely $\bar{N}_0$ and $\bar{E}_\mathrm{m}$, should be used when computing i_av. In Eq. 13, H is the altitude and H_0 and H_F the initial and final altitudes.

3.2. Optimal Impedance

As shown in Ref. [14], the normalized power dissipated by the impedance ($W = RI_C^2$ with I_C the cathode current) reads

$$\frac{W}{\sigma_\mathrm{t} A_\mathrm{t} E_\mathrm{m}^2 L^*} = w(\phi_\mathrm{C}, \xi_\mathrm{t}, z). \tag{14}$$

Such a power is a function of the dimensionless parameters in Eq. (6) (the explicit mathematical model for function w can be found in Ref. [14]). Since z also appears in the average current in Eq. (5), it is clear that the impedance should be designed carefully in order to harvest a good amount of power and achieve short deorbit times. In this work, we study the impedance that maximizes the power and use it to find the deorbit time and verify that it is reasonable (on the order of a few months). For $\phi_\mathrm{c} = 0$, such optimization problem was already investigated [14, 13, 1, 16] and the impedance that maximizes the power is

$$z_\mathrm{opt} = \xi_\mathrm{t}, \quad \xi_\mathrm{t} \gg 1 \tag{15}$$

$$z_\mathrm{opt} = \frac{4}{5} \left(\frac{5}{3} \right)^{3/2} \frac{1}{\xi_\mathrm{t}^{1/2}}. \tag{16}$$

In our work we found the optimal value numerically for $\phi_\mathrm{C} \neq 0$, too. Figure 4 shows the normalized optimum impedance versus ξ_t for three values of the normalized potential drop at the cathode. For convenience, the analytic expressions in Eqs. (15)–(16) (for the case of $\phi_\mathrm{C} = 0$) were also plotted using dashed lines.

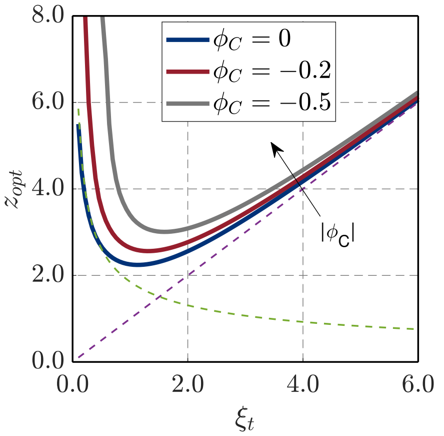

Figure 4. Normalized optimal impedance versus the normalized tether length for several potential drops at the cathode (solid lines). The dashed lines correspond to the analytical laws given by Eqs. (15)–(16).

To conclude this short analysis of the electric model of a bare tether with an impedance, Fig. 5 shows the normalized average current (left axis and blue curves) and the normalized power (right axis and red curves) versus ξ_t when the impedance is equal to z_{opt}. The curves are shown for three values of the normalized potential drop at the cathode. The power increases with ξ_t, whereas i_{av} is saturated due to ohmic effects. The results shown in Ref. [16] for $\phi_C = 0$ are recovered. For instance for $\phi_C = 0$, it can be observed that for $\xi_t \gg 1$ and at maximum power, $i_{av} = 0.5$. This value corresponds indeed to the asymptote of i_{avopt} in Figure 5, though it should be noted that our normalization differs, as we use L^* instead of Lt for power normalization.

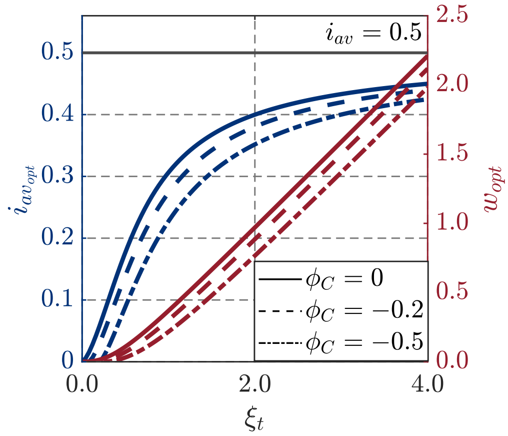

Figure 5. Normalized average current (left) and power (right) versus ξ_t for $z = z_{opt}$. Results for three normalized potential drop at the cathode are shown.

3.3. EDTs Performance

This section studies a few scenarios for different masses and inclinations of space objects and analyzes the deorbit time and the harvested power. The most promising cases were selected by analyzing the database from the previous chapter, focusing on orbit inclinations and masses that are promising for reaching good performances in terms of power harvesting. By analyzing Figure 1, it was found that the promising cases are within the mass ranges of 270–330 kg, 450–510 kg, and 690–750 kg. Within these ranges, the three satellite groups shown in Table 1 were identified. They are the Earth observation satellites Yaogan Weixing launched by China and the Russian Cosmos. These cases should be taken as example to illustrate the performance of the EDTs.

Table 1. Mass (M_s), orbit inclination (i), actual altitude (H) and number of objects for the selected scenarios (N).

Case	M_s [kg]	i [deg]	H [km]	N
Yaogan Weixing	300	35	500	52
Yaogan Weixing	500	35	580	29
Cosmos	743.31	74	780	51

In the analysis, the EDT system mass is assumed to be negligible with respect to the mass being removed and, for each altitude, the impedance is adjusted to be equal to the optimal, i.e. z_{opt}. We considered a tape-like EDT with cross-sectional area $A_t = 2.5\,\text{cm} \times 50\mu\text{m}$, made of Aluminum ($\sigma_t = 3.546 \times 10^7/\Omega\text{m}$), $C_D = 2$, $A_S/M_S = 0.01\ \text{m}^2/\text{kg}$. The tether length was varied in the parametric analysis. The orbits are circular and, independently of the altitudes identified in Table 1, we provide results for $H_0 = 800$ km and $H_F = 380$ km.

The deorbit time and the harvested power were computed from Eq. (13) and (14), where to evaluate the power we used z_{opt}, and for ϕ_C and ξ_t we used the environmental model and assumptions explained in the previous section.

Figure 6 shows the optimal harvestable power versus the altitude for three tether lengths and 35° of inclination. Even with a tether length of 1 km, the amount of power reaches approximately 100 W at an altitude of 380 km. For a tether length of 3 km, the power is above 180 kW at 800 km altitude and reaches values above 600 W at the final altitude. The instantaneous harvestable power depends on plasma density, and therefore, on the illumination conditions. Higher plasma density occurs in the day side. However, unlike solar panels that only harvest power when illuminated by the sun, the EDT system can provide power during eclipse. This feature, together with the results of Fig. 6, suggests that EDTs are a promising technology for providing power while deorbiting in low-inclined orbits.

Figure 7 shows a similar analysis but for 75° of inclination and tether lengths equal to 3, 4 and 5 km. Although the tether lengths are equal or larger than the ones in Figure 6, the amount of power is significantly lower. Nonetheless, values between tens to one hundreds of Watts can be harvested, which are interesting values taking into account the cost of space solar panels and their related deployment mechanism. This result suggests that this inclination is likely the limit beyond which spinning the tether would become necessary to harvest large amount of power instead of using an EDT along the local vertical. Such analysis is beyond the scope of this work.

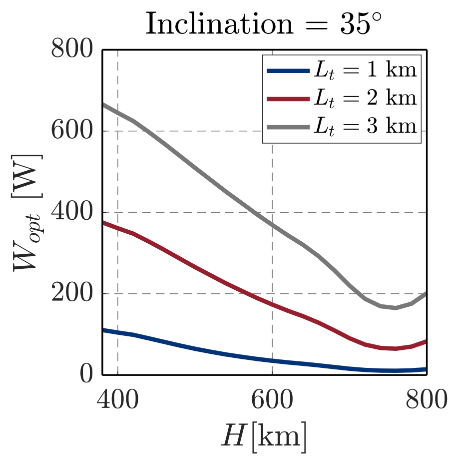

Figure 6. Optimal harvested power versus the altitude at 35° of inclination for different tether lengths.

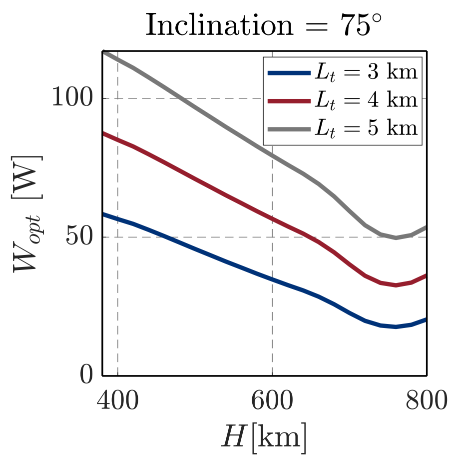

Figure 7. Optimal harvested power versus the altitude at 75° of inclination for different tether lengths.

For these conditions of optimal harvestable power, a study on the required decay time was conducted. Figure 8 shows the deorbit time versus the tether length for 35° of inclination. It is on the order of approximately three months for a 1-km tether in the case of 300 kg and around five months in the case of 500 kg. This makes this technology promising for missions requiring a short operational lifetime. Figure 9 the same quantities but for a harder case for the EDT because the inclination and the mass are both larger (75° and 750 kg). A longer tether length, between 3 and 5 km, is required to deorbit 750 kg within a similar time range as in the previous case.

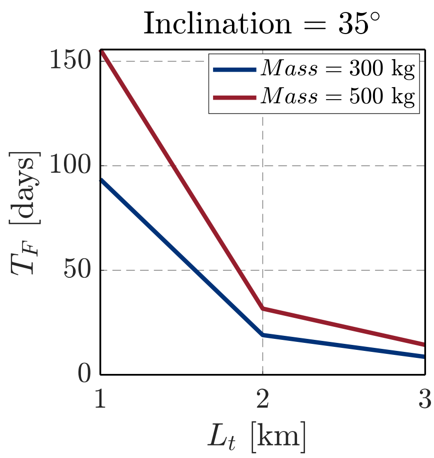

Figure 8. Deorbit time from 800 km of altitude versus tether length for the removal of 300-kg and 500-kg debris under optimal power harvesting conditions.

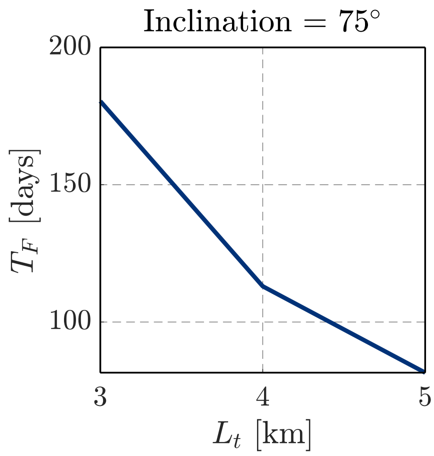

Figure 9. Deorbit time from 800 km of altitude versus tether length for the removal of 750-kg debris under optimal power harvesting conditions.

4. CONCLUSION

The potential of bare electrodynamic tethers (EDTs) for simultaneously enabling deorbiting and energy harvesting in Low Earth Orbit (LEO) was studied. By leveraging the conversion of orbital energy into electrical power, EDTs present a sustainable and propellant-free solution for space operations. The analysis has identified promising scenarios for which this technology can maximize its effectiveness, taking into account different debris masses and orbital inclinations.

The simple semi-analytical model proposed in the work allows to obtain quantitative information about the performance of the EDT, including deorbit time and harvested power. One of its essential components is the electrical model of the bare tether that has been analyzed to compute the optimum value of the impedance as a function of the normalized tether length and potential drop at the cathode. The normalize average current and power for optimal power harvesting conditions were also presented as a function of both parameters.

The application of the model to three selected scenarios revealed that EDTs can generate significant power while deorbiting space debris. The results are particularly promising at low-inclined orbits (35°) because relatively short EDTs can provide significant power (hundreds of Watts) with deorbit times in the order of a few months. For larger inclinations (75° in our analysis) the performance are lower, but still interesting taking into account the actual cost of solar panels and the fact that they cannot provide power during eclipses. Moreover, the current analysis was focused on tether configurations aligned with the local vertical. For high inclined orbits, better performances could be achieved by using spinning EDTs. Future research will explore this aspect, further refining the feasibility and performance of EDT-based systems for space debris mitigation and power generation.

ACKNOWLEDGMENTS

This work was supported by the European Union's Horizon Europe Research and Innovation Programme (No 101161603, E.T.COMPACT project).

REFERENCES

1. Bombardelli, C., Lorenzini, E. C., & Sanmartin, J. R. (2009). Jupiter power generation with electrodynamic tethers at constant orbital energy. *Journal of Propulsion and Power*, **25**(2), 415-423
2. Bombardelli, C., Herrera-Montojo, J., Iturri-Torrea, A., & Peláez, J. (2010). Space Debris Removal with Bare Electrodynamic Tethers. *Advances in the Astronautical Sciences.*
3. Bombardelli, C., Zanutto, D., & Lorenzini, E. (2013). Deorbiting Performance of Bare Electrodynamic Tethers in Inclined Orbits. *Journal of Guidance, Control, and Dynamics*, **36**(5), 1550-1556.
4. European Space Operations Centre (ESOC). (2024). DISCOS Web. Retrieved from `https://discosweb.esoc.esa.int/`. Accessed: 2024-12-20.
5. European Space Operations Centre (ESOC). (2024). DISCOS Web API Documentation v2. Retrieved from `https://discosweb.esoc.esa.int/apidocs/v2`. Accessed: 2024-12-20.
6. European Space Operations Centre (ESOC). (2024). DISCOS Web Statistics. Retrieved from `https://sdup.esoc.esa.int/discosweb/statistics/`. Accessed: 2024-12-20.
7. Forward, R. L., Hoyt, R. P., & Uphoff, C. W. (2000). Terminator Tether: A Spacecraft Deorbit Device. *Journal of Spacecraft and Rockets*, **37**(2), 187-196.
8. Hammond, Walter, Freeman, Scott, Nave, Mark, and Rupp, Charles. (1991). Jovian electrodynamic tether experiment. *29th Aerospace Sciences Meeting.*
9. McTernan, Jesse K., Bilén, Sven G., (2017). Embodied Energy Repurposing via Energy-Harvesting Electrodynamic Tethers, *Journal of Spacecraft and Rockets*, **54**(4), 789-795.
10. Sánchez-Arriaga, G., Borderes-Motta, G., and Chiabó, L. (2022). A code for the analysis of missions with electrodynamic tethers. *Acta Astronautica*, **198**, 471–481.
11. Sánchez-Arriaga, G., del Pino, A., Sharifi, G., Tarabini Castellani, L., García-Gonzaléz, S., Ortega, A., Cruces, D., Velasco, A., Orte, S., Ruiz, A., Matabuena, J., Martin, B., Wulfkuehler, J.-P., Drobny, C., Hertel, J., Nerger, R., Tajmar, M., Valmorbida, A., Chiodini, S., Polato, G., Anese, G., Brunello, A., Colombatti, G., Lorenzini, E. C., & Hubert, D. (2024). The E.T.PACK-F Project: towards a flight-ready deorbit device based on electrodynamic tether technology. *AIAA SCITECH 2024 Forum.*
12. Sanjurjo-Rivo, M., & Peláez, J. (2011). Energy Analysis of Bare Electrodynamic Tethers. *Journal of Propulsion and Power*, **27**(1), 246–256. doi:10.2514/1.48168
13. Sanmartin, J. R., Ahedo, E., & Martinez Sanchez, H. (1990). An Anodeless Tether Generator. *In Proceedings of the AIAA Conference*.
14. Sanmartin, J. R., Martinez-Sanchez, M., & Ahedo, E. (1993). Bare wire anodes for electrodynamic tethers. *Journal of Propulsion and Power*, **9** (3), 353-360.
15. Sanmartin, J. R., and Lorenzini, Enrico C. (2005). Exploration of Outer Planets Using Tethers for Power and Propulsion. *Journal of Propulsion and Power*, **21**(3), 573-576.
16. Sanmartin, J. R., Lorenzini, E. C., & Martinez-Sanchez, M. (2010). Electrodynamic tether applications and constraints. *Journal of Spacecraft and Rockets*, **47** (3), 442–456.
17. Sanmartín, J. R., Sánchez-Torres, A., Khan, S. B., Sánchez-Arriaga, G., & Charro, M. (2015). Optimum sizing of bare-tape tethers for de-orbiting satellites at end of mission. *Advances in Space Research*, **56**(7), 1485–1492.
18. United States Strategic Command (USSTRATCOM). (2024). Space-Track. Retrieved from `https://www.space-track.org/`. Accessed: 2024-12-20.